Potential Effects of Amazon Deforestation on Tropical Climate

Edwin K. Schneider[1,2],

Meizhu Fan[1], Ben P. Kirtman[1,2], and Paul A. Dirmeyer[2]

[1]*George Mason University, Fairfax, Virginia*

[2]*Center for Ocean-Land-Atmosphere Studies, Calverton, Maryland*

email: schneide@cola.iges.org

July 2006

Abstract

The effects of Amazon deforestation have been simulated with a coupled general circulation model (GCM). The deforestation influences the global tropics, and in particular leads to significantly enhanced El Niño /Southern Oscillation (ENSO) variability. Diagnostic experiments with the coupled GCM are conducted to examine if changes in the coupled variability can be traced to the changes over the ocean found in an Amazon deforestation experiment done with climatological SST forcing of the atmospheric GCM. The diagnostic experiments indicate that the mechanism for the enhanced ENSO variability is that changes in the land surface properties cause changes in the mean surface wind stress in the tropical Pacific. These wind stress changes destabilize the mean state of the coupled system, and ENSO variability increases.

The response of a simple Gill-type atmospheric model to the deforestation induced precipitation and surface temperature anomalies from the atmospheric GCM simulations is found. These indicate that the westerly wind stress anomalies over the far eastern Pacific are forced by the warmer surface temperatures over the deforested region rather than the reduced precipitation. Diagnoses with an intermediate coupled model of the tropical Pacific suggest that the wind stress anomalies over the far eastern Pacific are particularly important for destabilizing the mean state, and also that changes in the "weather noise" forcing are probably not important in enhancing the ENSO variability.

1. Introduction

We describe a long simulation of the response of the climate system to Amazon deforestation using a coupled general circulation model (CGCM), which indicates that Amazon deforestation could have a significant impact on ENSO (El Niño /Southern Oscillation) variability, and hence on the climate of the global tropics. Simulations of the potential effects of Amazon deforestation on climate have previously been made assuming that the sea surface temperature (SST) has no response (e.g. Henderson-Sellers and Gornitz 1984; Dickinson and Henderson-Sellers 1988; Nobre et al. 1991). The changes over land in these simulations are dramatic, including strong warming, exceeding 3°C, and pronounced changes in the precipitation patterns over the deforested areas. The effects are fairly consistent between different models, although uncertainties in the properties of deforested lands can lead to variations in the climate response (Dirmeyer and Shukla 1994, Sud et al. 1996). There has been some theoretical activity towards understanding the roles of the various mechanisms (e.g., Zeng and Neelin 1999).

There have been few publications reporting the effect of deforestation in coupled ocean-atmosphere models. Delire et al. (2001) have simulated the effects of Indonesian deforestation with a coupled atmosphere-ocean model of intermediate complexity, finding some effects on the surrounding ocean. Voldoire and Royer (2005) have conducted 20 year simulations of the effects of deforestation of the global tropics in a CGCM. Their simulation found statistically significant effects of deforestation on the mean climate over the tropical oceans, some of which will be described below. However, their simulations were not long enough to detect changes in coupled climate variability on ENSO time scales. Here, a simulation of the response of the climate system to

Amazon deforestation is carried out for 100 years, which is perhaps long enough to detect changes in ENSO variability.

In an experiment to examine the sensitivity of coupled climate variability to land surface processes, described by Bhatt et al. (2002), an unconstrained CGCM control simulation was compared with a simulation in which the soil moisture was globally specified to be that of the control climatology. The object was to reduce variability over land and to see the impact of this effect on the global climate. In the constrained soil moisture experiment, variability decreased over land as expected. Additionally, the tropical land surface had less precipitation (especially South America) and was cooler, and ENSO variability decreased. Hu et al. (2004) related the decrease in ENSO variability to an unphysical behavior which caused the tropical land surface to be an energy sink when the soil moisture was specified. Using an intermediate coupled model of the tropical Pacific (ICM) for diagnosis, they found that that the changes in the mean state over the tropical Pacific, in particular the mean wind stress, were probably more important than the decrease in the land surface variability in leading to the decrease in the ENSO variability. Although the mean state changes occurred because of problems with the experiment, the results suggest that there is a potential mechanism for changes in tropical land surface properties to affect tropical SST variability. Those results motivate the experiments described here, which evaluate the effects of a more physically based change to the land surface boundary conditions in simulations in which land surface energy conservation is not violated.

We find pronounced changes (significant at the 5% level) in the ENSO related SST variability between the deforested and control coupled simulations, but it is not clear

from the simulations alone by what mechanism deforesting the Amazon affects SST variability across the tropical Pacific. In the broadest sense, there are two mechanisms that have been suggested to influence ENSO variability. The first mechanism is that changes in the structure of the mean state cause changes in the stability of the coupled ocean-atmosphere system. Some potential effects of this mechanism are explored by Jin and Neelin (1993a, 1993b) and Fedorov and Philander (2001) in simplified models. The effects of mean state stability on ENSO variability are that 1) if the mean state is stable, ENSO variability will not occur spontaneously, and 2) if the mean state is unstable, ENSO variability will occur. In the unstable case, the variability can be either periodic or chaotic, depending on model formulation and parameters. Small changes in the external forcing of the system can then cause pronounced changes in the character of ENSO variability by forcing stable or unstable mean states and concurrent suppression or enhancement of the variability (e.g. the effect of changing the seasonal distribution of incident solar radiation in Clement et al. 2001). The second mechanism is stochastic forcing of the coupled system by noise associated with atmospheric fluctuations for which coupled dynamics are unimportant ("weather noise"). The response to the weather noise depends crucially on the stability of the mean state (Flügel et al. 2004 and references therein). When the mean state is stable or neutral, weather noise can stimulate ENSO variability where none would otherwise exist. When the mean state is unstable, the effects of noise can be more subtle.

In the COLA anomaly coupled CGCM, ENSO is a self sustaining oscillation whose properties are not crucially dependent on noise forcing, either from the atmosphere or the ocean. This has been shown using the "interactive ensemble" approach described

by Kirtman and Shukla (2002). In that study, an ensemble of six copies of the AGCM, all started from different initial conditions, is anomaly coupled to the OGCM (the "interactive ensemble" approach). Each copy of the AGCM sees the OGCM SSTA as it evolves, and the fluxes forcing the OGCM are the ensemble mean anomalies from the AGCMs. The interactive ensemble simulation procedure filters the atmospheric weather noise from the forcing of the OGCM. The ENSO variability in the interactive ensemble is nearly as large as in the anomaly coupled CGCM, with a similar spatial structure and period (2.5 to 3 years). If the weather noise forcing was crucial, the ENSO variance would have been reduced by a factor of 6, as noted by Wu et al. (2004). The interactive ensemble has been generalized to couple an ensemble of six copies of the OGCM with uncorrelated ocean internal noise to the AGCM ensemble. The SSTA seen by each of the AGCMs is then the ensemble mean from the OGCMs. The ENSO variability in the generalized interactive ensemble is essentially the same as that found with the single OGCM, showing that ocean internal noise forcing is not crucial for ENSO in the anomaly coupled CGCM either, and proving that it is a self-sustaining internal oscillation (see Kirtman et al., 2005).

In order to narrow down the mechanisms by which Amazon deforestation affects ENSO variability in our simulations, we have performed a number of additional experiments with the CGCM, the AGCM component of the CGCM, a simplified atmospheric model, and an ICM. Diagnostic experiments are carried out with the CGCM to determine whether changes in the mean atmospheric fluxes over the ocean induced by the deforestation in the absence of atmosphere-ocean coupling can explain the change in ENSO in the coupled system. The CGCM diagnosis indicates that seemingly small

changes in the climatological wind stress over the tropical Pacific induced by the deforestation are able to stimulate the enhanced ENSO variability and associated larger changes in the mean state, while tropical Pacific heat flux changes induced by the deforestation are not. Diagnosis with the simplified atmospheric model point to regionally specific roles of the surface warming and deep convective heating changes due to deforestation in producing the wind stress changes. Diagnoses using the ICM point to enhanced instability of the mean state near the South American coast as the underlying mechanism, and suggest that changes in the weather noise forcing are not important.

We describe the CGCM and diagnostic models in Section 2, results from the CGCM deforestation experiment, including biases in the control simulation in Section 3, the CGCM diagnosis in Section 4, the simple model diagnoses in Section 5, and conclusions in Section 6.

2. Models and experimental design

The coupled GCM used in the experiments is the COLA anomaly coupled GCM (Kirtman et al. 2002). Brief descriptions of the atmospheric GCM, ocean GCM, land model, anomaly coupling strategy, and experimental design are given in this section.

a. Atmospheric GCM

The atmospheric model is version 2 of the COLA AGCM. The model physics is described in Schneider (2002). The dynamical core is from the NCAR(National Center for Atmospheric Research) CCM3 (Community Climate Model version 3), now known as CAM1 (Community Atmospheric Model version 1), described in Kiehl et al. (1998). The horizontal discretization is spectral and the vertical coordinate is sigma (pressure divided by surface pressure), and the resolution for this investigation is T42 with 18 vertical

levels. The parameterization of the solar radiation is after Briegleb (1992) and terrestrial radiation follows Harshvardhan et al. (1987), and includes a realistic evolution of the Earth's orbital parameters (Marx 2001). The deep convection is an implementation of the relaxed Arakawa–Schubert scheme of Moorthi and Suarez (1992) described by DeWitt (1996). The convective cloud fraction follows the scheme used by the NCAR CCM (Kiehl et al. 1994; DeWitt and Schneider 1996). There is a turbulent closure scheme for the subgrid-scale exchange of heat, momentum, and moisture as in Miyakoda and Sirutis (1977) and Mellor and Yamada (1982, level 2.0).

b. *Ocean GCM*

The ocean model is the Geophysical Fluid Dynamics Laboratory (GFDL) Modular Ocean Model version 3 (MOM3), described by Pacanowski and Griffies (1998), a finite-difference treatment of the primitive equations of motion using the Boussinesq and hydrostatic approximations in spherical coordinates. The zonal resolution of the ocean model is 1.5°, and the meridional grid spacing is 0.5° between 10°S and 10°N, gradually increasing to 1.5° at 30°N and 30°S and fixed at 1.5° in the extratropics. There are 25 levels in the vertical with 17 levels in the upper 450 m. The domain is that of the World Ocean between 74°S and 65°N. The coastline and bottom topography are realistic except that ocean depths less than 100 m are set to 100 m and the maximum depth is set to 6000 m. The artificial high-latitude meridional boundaries are impermeable and insulating. The vertical mixing scheme is the non-local K-profile parameterization of Large et al. (1994). The horizontal mixing of tracers and momentum is Laplacian. The momentum mixing uses the space-time dependent scheme of Smagorinsky (1963) and the

tracer mixing uses Redi (1982) diffusion along with Gent and McWilliams (1990) quasi-adiabatic stirring.

c. Land model

The land surface model is an updated version of the simplified Simple Biosphere model (SSiB; Xue et al. 1991, 1996) as described by Dirmeyer and Zeng (1999). SSiB is a typical second-generation land surface scheme (closed energy and water budget but no simulation of the carbon cycle) and has three soil layers: a thin surface layer of fixed depth, a root zone of 0.5 to 2.5m depending on vegetation type, and a deep recharge zone. The surface energy budget of the canopy and soil are treated separately. Independent data sets of global vegetation types and soil parameters are used, with a specified mean annual cycle of vegetation properties based on observations. A sub-grid precipitation interception scheme and canopy interception/re-evaporation are incorporated for more realistic surface hydrology. However, recharge of soil moisture from the water table below the third soil layer is not included, nor is surface liquid water storage (e.g. from floodplain inundation).

d. Coupling

The CGCM uses the anomaly coupling strategy (closely related to flux correction), which is applied at the air-sea interface in order to keep the control climate close to the observed (Kirtman et al. 1997; Kirtman et al. 2002). All current state-of-the-art CGCMs suffer to some extent from severe tropical biases and unrealistic characteristics of ENSO variability. These biases are described for the COLA CGCM in Schneider (2002) and Kirtman et al. (2002). The rationale behind the use of anomaly coupling is that the coupled variability, especially with regard to ENSO, is expected from

the theoretical studies cited in the Introduction, as well as many others, to depend crucially on the simulation of the climatological mean state, including the annual cycle. A realistic simulation of the climatological states of the atmospheric and ocean and the fluxes between them is then a necessary but not sufficient condition for a realistic simulation of the ENSO variability. Anomaly coupling is a partial fix that addresses only SST and the surface fluxes, and greatly reduces the biases in these, but does not address the underlying causes of the biases in the models' physics and numerics, which are undoubtedly still important in biasing the internal atmosphere and ocean climatologies as well as the anomalies.

In anomaly coupling, the atmospheric GCM is forced by the observed climatological SST plus the anomaly of the ocean model's SST from the OGCM climatology. Similarly, the SST is the OGCM response to the observed climatological fluxes of heat, momentum and freshwater plus the atmospheric anomalous fluxes with respect to the AGCM climatology. The ocean and atmosphere models exchange daily mean fluxes of heat, momentum, and freshwater and SST once a day. No additional empirical corrections are applied to any of the exchanged anomalies. Also, there is no coupling of simulated terrestrial runoff to the ocean model.

This coupling constrains the CGCM climatological SST, including the annual cycle, as seen by the atmosphere, to be close to the observed in control simulations, and similarly constrains the climatological wind stress, heat flux, and fresh water flux as seen by the ocean. Note that the SST produced by the ocean is not constrained to be close to the observed. Even if the fluxes forcing the ocean have no biases, the OGCM will produce biases in the SST due to inaccuracies in the ocean model, and similar comments

apply to the atmospheric fluxes. The variability of the CGCM is not constrained explicitly by the anomaly coupling.

The component model climatologies are defined by separate uncoupled extended simulations of the ocean and atmospheric models. In the case of the atmosphere, the model climatology is computed from a 30-yr (1961–90) integration with observed specified SST. This SST is also used to define the observed SST climatology. The observed SST dataset is described in Smith et al. (1996). In the case of the ocean model SST climatology, an extended uncoupled ocean model simulation is made using 30 yr of 1000-mb NCEP–NCAR reanalysis winds. The NCEP–NCAR winds are converted to a wind stress following Trenberth et al. (1990). As with the SST, this observed wind stress product is used to define the observed momentum flux climatology. The heat flux and the freshwater flux in this ocean-only simulation are parameterized using damping of SST and sea surface salinity to observed conditions with a 100-day timescale. The heat and freshwater flux ‘‘observed’’ climatologies are then calculated from the results of the extended ocean-only simulation.

The anomaly coupling framework provides a useful tool for carrying out controlled diagnostic experiments, such as those that are described in Sec. 5. Changes made in the climatological fluxes provided to the ocean will produce SST anomalies that project on the climatological fields, effectively producing a new climatological SST. This could then lead to changes in the variability, and perhaps further changes in the climatological SST.

e. Experimental procedure

The control simulation, CONTROL, started with the astronomical parameters of Jan. 1, 2000 after a 50 year spin-up of the ocean made with climatological stresses. The Amazon deforestation experiment DEFOREST was initialized at the Jan. 1, 2100 state of CONTROL. In DEFOREST, the vegetation in the Amazon region (shaded area in Fig. 3b), tropical rain forest, was replaced by the savanna vegetation type. This change results in a decrease of root depth from 2.5 m to 1.0 m, a reduction in canopy height from 35m to 1m with a concomitant decrease in roughness length and displacement height, an overall decrease in leaf area index and greenness, increased net surface albedo, and the introduction of intra-annual variations of vegetation properties synchronized with the mean wet and dry seasons. The replacement area represents a complete deforestation of the Amazon. This extreme and probably unrealistic scenario is appropriate for a first sensitivity and mechanistic study of the potential effect on the coupled climate system. The period of the analysis is from Jan. 1, 2100 to Dec. 31, 2199 for both simulations. The 5% level is chosen to test for significance. Names and descriptions of CGCM experiments are listed in Table 1.

f. Diagnostic models

The atmospheric component of the model of Zebiak and Cane (1987) is used to examine the steady atmospheric response to forcing by heating. This model is based on the work of Gill (1980). The model is also used to find the response to imposed surface temperatures, using the isomorphism between the Gill model and the Lindzen and Nigam (1987) model described by Neelin (1989).

We also use an ICM of the tropical Pacific for diagnosis (Kirtman 1997, Hu et al. 2004). It consists of a statistical atmosphere coupled to the ocean component of the model of Zebiak and Cane (1987). The ocean model domain is 130°E-84°W, 19°S-19°N. The SST equation determines the evolution of the SSTA, essentially linearized about the climatological annual cycle of SST, thermocline depth, and current. The statistical atmosphere is derived by simultaneous regression of the 1964-94 observed NINO3 SSTA onto the Florida State University analyzed surface wind stress (Goldenberg and O'Brien, 1981). The wind stress thus has a time independent spatial structure. The heat flux is chosen to damp the SSTA. Parameters and basic state fields are chosen to model the observed tropical Pacific. With these choices, the ENSO variability in the ICM is exactly periodic with a period of about four years. The ICM is not entirely consistent with the CGCM, since the statistical model is of the real atmosphere rather than the CGCM atmosphere, the thermocline properties are taken from the real ocean, rather than the CGCM ocean, and the eastern boundary of the ICM ocean basin is at a constant longitude rather than following the South American coastline. However, there is some correspondence between the responses of the ICM and the CGCM to similar anomalous forcing, as will be discussed below. The ICM diagnoses should then be interpreted as suggestive rather than definitive.

3. Results

In the following, we will refer to the SST variability in the equatorial Pacific as "ENSO." Properties of ENSO in the CONTROL and DEFOREST are summarized by the variability of NINO3.4. The rainfall and surface temperature simulation of CONTROL in

the Amazon region is compared to the observed and to DEFOREST. Then the geographical distribution of the response to the deforestation is described.

a. NINO3.4 SSTA

Figure 1 shows 100 years of monthly mean observed HadSST (Rayner et al., 1996; top panel) and simulated (bottom panel) NINO3.4 SST variability. The standard deviation of the NINO3.4 SSTA is 0.59°C in CONTROL, which is about 20% smaller than the 0.75°C value found in observations over 1900-1999 (but closer to the observed value of 0.66°C over the 1900-1970 period). The standard deviation of the NINO3.4 SSTA in DEFOREST is 0.66°C. The difference between the CONTROL and DEFOREST variances is significantly different from zero at the 5% level. The number of degrees of freedom used in the significance level calculation (257) was estimated from the autocorrelation time of the simulated NINO3.4 SSTA in CONTROL (approximately 6 months).

The power spectra of the NINO3.4 SSTA have also been calculated (not shown). The observed spectrum has a well known single prominent peak with a period of about 4-5 years. The simulations have most of their power at interannual to decadal periods, with peaks near 3 and 8 years in CONTROL and near 3 and 6 years in DEFOREST. There do not appear to be significant differences between the ENSO periods in CONTROL and DEFOREST.

b. Land surface biases and response

While anomaly coupling constrains the CONTROL simulation climatological SST to be close to the observed, the land surface is unconstrained by artificial corrections, and can therefore develop biases. The climatological annual cycles of the

precipitation and surface air temperature from the simulations and analyses of observations over the land region 80°W-40°W and 15°S-8°N, which contains the deforested region, are shown in Fig. 2. The analysis climatologies are obtained from CMAP (CPC Merged Analysis of Precipitation**)**, 1979-2003 (Xie and Arkin 1996) for precipitation, and from CAMS (Climate Anomaly Monitoring System), 1946-2003 (Ropelewski et al. 1985) for surface air temperature. It is obvious that CONTROL has significant biases, in that precipitation (Fig. 2a) is too low (annual mean 2.3 mm day^{-1} for CONTROL, 5.0 mm day^{-1} for CMAP), and surface air temperature (Fig. 2b) too high (annual mean 25.6°C for CONTROL, 24.9°C for CAMS). The biases are especially pronounced in the rainy seasons, with CONTROL precipitation only 1/3 of CMAP, and surface air temperatures too warm by almost 2°C. These COLA model biases have been discussed by Misra et al. (2003) for the COLA AGCM, and are similar to those found in the coupled simulations described by Voldoire and Royer (2005). These biases need to be kept in mind in interpreting the results.

Amazon deforestation leads to a reduction in the area mean precipitation (annual mean reduction 0.3 mm day^{-1}) and a warming in the surface air temperature (annual mean higher by 1.8°C) for DEFOREST relative to CONTROL, as shown in Fig. 2.

c. Structure of anomalies

The ENSO simulation of CONTROL was compared to observations and to a directly coupled simulation in Kirtman et al. (2002). While the amplitude of the equatorial SST anomalies is reasonable in CONTROL, the strong SST anomalies (Fig. 3a) are too narrowly confined to the equatorial region, especially in the eastern Pacific, and also extend too far into the western Pacific. Without anomaly coupling, Kirtman et

al. (2002) found that the ENSO structure was too strongly confined to the eastern Pacific, due to biases in the mean state.

A comparison of CGCM simulations (Latif et al. 2001) found that an earlier version of this model (the baseline COLA CGCM described in Schneider 2002) produced one of the better simulations of the observed ENSO period of approximately four years. The current version differs from the previous one primarily in that in the current version 1) the AGCM horizontal resolution is T42 (previously T30), 2) the OGCM is MOM3 (previously MOM2) and has different physical parameterizations but similar resolution.

Figure 3b shows the sensitivity of the SST variability. Deforestation leads to enhancement of model's ENSO-related SST anomalies in the equatorial Pacific by about 20% in the region of strongest variability (significantly different from zero at the 5% level). SST variability is also enhanced in the tropical Atlantic.

Along with the changes in SST variability, the mean SST (Fig. 3c) in the equatorial and south-equatorial eastern Pacific also changes. This structure of the mean SST change, with warming in the equatorial central and eastern Pacific, has also been found in some simulations of the effects of increasing greenhouse gases, where it has been referred to as “El Niño-like” warming (Meehl and Washington, 1996) because it resembles the structure of SST anomalies during an El Niño event (warm phase of ENSO). The atmospheric mean state also changes toward a more El Niño-like configuration, with displacement of precipitation from the western towards the central Pacific and a more westerly surface wind stress in the central and eastern equatorial Pacific (Fig. 3d). The Amazon region is substantially drier in the deforested simulation, as would be expected from the specified SST deforestation simulations. The small scale

structures in the unsmoothed precipitation anomalies over South America are fixed to surface features. This spatially spotty behavior is a property of the COLA AGCM. The equatorial Atlantic is slightly cooler in DEFOREST, coinciding with more easterly surface wind stress and reduced precipitation.

Warm anomalies in the eastern Pacific are also shown by Voldoire and Royer (2005) in DJF and JJA (their figures 9b and 10b, respectively). They also find a similar pattern of annual mean precipitation anomalies (their Fig. 13d: positive in the central and eastern Pacific, negative in the Atlantic, and negative over the Amazon.

4. Diagnostic GCM simulations

It is difficult to determine cause and effect in the coupled simulations, since coupled feedbacks between the atmosphere and ocean have an important influence in the results of the experiments. It would seem reasonable to hope that the underlying cause for the changes in the CGCM is present in AGCM control and deforestation simulations forced by climatological SST. We have devised a procedure incorporating the AGCM deforestation response into the CGCM with CONTROL vegetation in order to test which, if any, of the deforestation-induced changes in surface flux is responsible for the changes in the ENSO variability.

a. AGCM forced by climatological SST

We conducted 28 year control and deforestation simulations using the AGCM forced by the climatological annual cycle of SST, 1971-2000, from the Smith et al. (1996) analysis. The biases in the AGCM control simulation are close to those found in the CGCM CONTROL, which is expected since the CONTROL SST is bias-corrected to be close to the HadSST climatology. The sensitivities of surface temperature and

precipitation over the land region as in Fig. 2 are close to those found with the CGCM. Changes in the fluxes of heat, momentum, and fresh water over the oceanic regions were saved for use in the diagnostic coupled simulations described below. The sensitivity of the "weather noise" in the surface fluxes to deforestation was also evaluated in the climatological SST simulations for use in diagnostic simulations. The weather noise for a simulation was taken to be the variability in the surface fluxes after its climatological annual cycle was removed.

Strong warming over the Amazon is found, as in previous studies such as those referred to in the Introduction. Deforestation leads to generally decreased precipitation in the Amazon, but enhanced precipitation in the surrounding regions (Fig. 4). The precipitation sensitivity over the Amazon is very similar to that found in the CGCM in DEFOREST minus CONTROL, including the small scale features. This is a demonstration that the precipitation sensitivity of the coupled simulation is highly deterministic and predictable, and not "noise," despite the lack of spatial coherence. It also shows that the land response is not changed by coupling to the ocean, as in Voldoire and Royer (2005). Deforestation produces the change in the surface wind stress over the ocean as shown in Fig. 4. There are easterlies over the tropical central Pacific, but with a stronger magnitude off than on the equator. Also, there are equatorial westerlies in the far eastern Pacific connecting cyclonic vortices to the north and south of the equator. The wind stress anomalies are substantially weaker than those found in the coupled simulation. Aside from the amplitude, the climatological SST forced and CGCM wind stress patterns have similar structures in the low latitude eastern Pacific as well as the western Atlantic. There is also increased heat flux into the ocean in the eastern Pacific

(not shown). The changes over the ocean produced by the Amazon deforestation in the uncoupled AGCM simulation will be referred to as the "deforestation forcing" of the ocean.

b. Diagnostic CGCM simulations

The annual mean deforestation forcing is then added to the fluxes provided to the ocean in CGCM simulations with CONTROL vegetation (i.e. without Amazon deforestation). This flux correction represents the forcing of the ocean by the deforestation before the coupled feedbacks come into play. The CGCM simulations test whether the coupled feedbacks will then amplify the deforestation forcing and produce the effects similar to those seen in DEFOREST. Two experiments were performed, one using only the heat flux deforestation forcing, and the other with only the momentum flux deforestation forcing (denoted WIND). Both experiments applied the deforestation forcing globally. Simulations of 40 years were carried out from identical initial conditions and the final 30 years were analyzed. When the heat flux shown was added to the climatological heat flux, there was no significant change in the mean state SST or ENSO variability. However, adding the deforestation forcing mean wind stress changes of Fig. 4 leads to the WIND anomalies relative to CONTROL shown in Fig. 5.

In the tropical Pacific the WIND anomalies are very similar to those found in DEFOREST. There is enhanced equatorial SST variability in both the central Pacific and near the South American coast (Fig. 5a). The anomalies are actually somewhat stronger than those in DEFOREST, so that despite the reduction in the length of simulation and degrees of freedom in WIND, the significant regions have similar areas in Figs. 3b and 5a. Changes in the mean state also closely resemble those found in DEFOREST. There

are El Niño-like mean SST changes in the Pacific and cooling in the Atlantic (Fig. 5b) similar to those shown in Fig. 3c, although changes in the mean SST are more closely confined to the equator than those found in DEFOREST. Annual mean precipitation is higher over the central and eastern equatorial Pacific and lower in the western equatorial Pacific. Changes in the wind stress (Fig. 5c, arrows), have similar structure and magnitude to those shown in Fig. 3d. Changes in the tropical Atlantic (Fig. 5) mean state and variability are also induced by both deforestation wind stress forcing in WIND and Amazon deforestation in DEFOREST.

Note in Fig. 5c that the annual mean precipitation changes over the Amazon are very small in WIND. The vegetation is the same in both WIND and CONTROL. Only the forcing of the ocean is different. The lack of change in Amazon precipitation induced by forcing the over the ocean in another demonstration that there is little feedback back to the land from the changes in the ocean mean state.

These results suggests elements of a mechanism for the enhanced SST variability and the mean state changes. Amazon deforestation directly causes small but physically significant changes in the mean wind stress over the equatorial Pacific. These changes in the mean wind stress destabilize the coupled system, leading to enhanced SST variability and, through coupled feedbacks, larger changes in the structure of the coupled mean state.

5. Diagnoses with simpler models

There are several gaps in the argument connecting deforestation → mean wind stress forcing → enhanced ENSO variability that need to be filled in. In particular:

a. How does the deforestation produce the deforestation wind stress forcing?

b. Which aspects of the deforestation wind stress forcing are important to initiate the changes in the coupled system?

c. What is the role of noise forcing?

It is also important to evaluate the robustness of the various mechanisms, as it is possible that at least some aspects of the results may be model dependent, especially given the biases in the model's mean state. These issues are addressed below.

a. Surface wind response to Amazon deforestation

The WIND experiment isolates an important cause of the enhanced ENSO variability in DEFOREST to be the annual mean surface wind stress anomalies produced by deforestation as identified in the AGCM-only deforestation simulation. As mentioned in Sec. 4a, the annual mean surface wind stress anomalies produced in the AGCM-only deforestation simulation has equatorial easterlies in the Atlantic and anticyclonic circulations symmetric about the equator, with equatorial westerlies, in the far eastern Pacific. This structure is reminiscent of surface response of the Gill (1980) model expected for an isolated heat source located in equatorial South America.

In order to further analyze this response, the simple Gill-type steady linear atmospheric model described in Sec. 2f was used to diagnose the surface response to the precipitation (representing convective heating) and surface temperature anomalies from the AGCM-only simulation. Following Neelin (1989), the model used for the response to heating has mechanical and thermal damping coefficients of $(2\ \text{days})^{-1}$, while thermal damping time is reduced to $(30\ \text{minutes})^{-1}$ for surface temperature forcing to represent the Lindzen and Nigam (1987) boundary layer model. Also, the equivalent depth is reduced by a factor of ten for surface temperature forcing, which represents a boundary

layer depth of 3000 m. While the Lindzen and Nigam model has been used extensively when forced by SST, we are not aware of applications diagnosing the atmospheric response to land surface temperatures. However, the argument used to derive the model, that the surface pressure "boundary layers" in the tropics, and that the appropriate boundary layer depth is more or less a constant throughout, which is justified both theoretically from Ekman layer theory (Schneider and Lindzen, 1976) and observationally, applies equally well over ocean or land.

Note that over land, specific humidity variations may be important in evaluating pressure gradients. Then it is appropriate to use virtual rather than absolute surface temperature to force the model, but we have not done that here.

The surface wind responses of the diagnostic model to anomalies found in the AGCM-only deforestation minus control simulations are shown in Fig. 6. The figure shows the normalized responses (both u and v normalized independently) to deforestation minus control atmospheric heating anomalies (Fig. 6a), taken proportional to the annual mean precipitation anomalies, and to deforestation minus control annual mean surface temperature anomalies (Fig. 6b). The deforestation minus control surface wind stress anomalies found in the AGCM simulations are also shown (Fig. 6c), where the stresses on land have been multiplied by 0.1 and those on ocean by 10 in order for the vector lengths over land and ocean to be comparable. Zonal means are removed.

Since there is a reduction of precipitation over the Amazon due to deforestation, the precipitation forced surface winds diverge there in response (in the Gill model this is seen from the u-component). Additionally, the surface winds are easterly over the equatorial Pacific and westerly over the equatorial Atlantic near South America. This

response appears to coincide reasonably well with the divergent AGCM response over land, and possibly also in the Atlantic south of the equator. The AGCM response to the west of 110°W is also similar to the response to the precipitation forcing. However, the response to precipitation cannot explain the westerly response to deforestation in the eastern Pacific or the easterlies in the equatorial western Atlantic found in the AGCM simulations.

Consider next the response to the increased Amazon surface temperature due to the deforestation in Fig. 6b. The surface temperature forcing over the ocean is zero, since both the control and deforestation AGCM-only simulations are forced by climatological SST. Thus the forcing is due only to the land surface temperature response, and the response over the oceans is entirely a remote response to the land surface temperature forcing. In contrast to the response to heating, this response is convergent over the land. Also, the response is westerly over the eastern equatorial Pacific and easterly over the western equatorial Atlantic, similar to the AGCM response.

The simple model diagnosis then suggests that the wind response over the equatorial eastern Pacific can be attributed to the remote response to the land surface temperature anomalies caused by the deforestation. This response cannot be explained by the response to condensation heating (e.g. deep convection), since that response has the wrong sign. It is reasonable to expect that this westerly response should be a robust feature of AGCM-only Amazon deforestation simulations, as far as the warming response to deforestation is robust.

Other features of the simple model diagnosis are also worth noting. Using a linear model to diagnose AGCM simulations, Dewitt et al. (1996) found that boundary layer

convergence forced by condensation heating and that forced by boundary layer diffusion (corresponding to surface temperature forcing here) were 180 degrees out of phase over land, but reinforced each other over ocean. Here, we have found the same result over land from our linear model diagnosis. The mechanism for this relationship in the AGCM clearly involves feedbacks between precipitation and surface temperature that are present over land (small heat capacity, evaporation dependent on soil moisture) but not ocean (large heat capacity, potential evaporation). The diagnosis indicates that over the Atlantic, the easterly responses to both forcings reinforce south of the equator, with asymmetry of the zonal wind about the equator attributable to the precipitation forcing. In the Atlantic north of the equator, the responses compete, with the surface temperature forcing winning out near the coast. The response to surface temperature decays with increasing distance from South America, while the response to deep convective heating does not. This is in part due to the smaller equivalent depth (and smaller scale of influence) appropriate for the surface temperature forcing interpretation, and in part due to the localization of the surface temperature forcing to South America.

b. ICM response to deforestation mean wind anomalies

Adding the annual mean wind stress anomaly of DEFOREST (Fig. 3d) to the climatological wind stress forcing in the ICM leads to a pronounced enhancement of its ENSO variability. This indicates that the ICM interprets the changes in the CGCM mean wind as being associated with a more unstable mean state. Since the DEFOREST annual mean wind anomalies have already been amplified by coupled feedbacks from those produced in the AGCM-only simulation, this result is not directly relevant to

understanding the cause of the larger ENSO variability, but it provides some justification for using the ICM as a tool for preliminary testing of mechanisms, as in Hu et al. (2004).

The analogous experiment to WIND was conducted with the ICM. That is, the AGCM-only deforestation minus control annual mean wind stress anomalies were added to the climatological background state. The result of this experiment was that the ENSO variability was eliminated, that is the mean state became stable, which does not agree with the results from the CGCM experiments. It is clear at least from this result that the ICM mean state is close to a boundary between stable and unstable regimes, and lies on the unstable side. Additional experiments were conducted applying the deforestation annual mean wind stress anomalies from various geographical regions. When the region was taken to be 90°-84°W and 5°-11°S, on the edge of the ICM domain near to the South American coast (close to the NINO1 region 90°-80°W and 5°-10°S), the ICM produced enhanced ENSO variability. The ENSO variability did not change when the forcing was applied in corresponding region to the north of the equator. Thus, while the ICM results are not entirely consistent with those from the CGCM, the ICM suggests that the region between the South American coast and 90°W and south of the equator, some of which is outside the domain of the ICM, may be a key region for destabilizing the coupled system via the deforestation-induced mean wind changes. The results from the linear atmospheric model indicate that surface temperature anomalies produced by Amazon deforestation have their strongest influence in this region, which is at least consistent with this conjecture.

c. The role of noise forcing

It is also possible that enhanced stochastic forcing by atmospheric "weather noise" could be forcing stronger low frequency ENSO variability, in a variant of the random walk mechanism (i.e. Flugel et al. 2004). The enhanced ENSO variability could then lead to an El Niño-like warming by acting as a mixing agent and smoothing the east-west SST gradient, which in turn would force El Niño-like changes in the atmospheric wind stress and precipitation fields (Schopf and Burgman 2006). This possibility was tested by forcing the ICM with climatological mean state with the "weather noise" wind stress produced in the deforestation and control climatological SST AGCM-only simulations. The weather noise was taken to be the time series of the AGCM wind stress with the annual cycle removed. The result from this experiment was negative: as in the ICM diagnosis in Hu et al. (2004) there was no difference in ENSO variability between the two simulations.

6. Conclusion

Some of the sensitivities of the COLA anomaly coupled CGCM to Amazon deforestation were described. Effects on the Amazon rainfall and surface temperature are similar to those found in AGCM-only simulation. Over ocean the Amazon deforestation leads to enhanced ENSO variability and annual mean warming in the eastern equatorial Pacific.

According to our diagnostic simulations, the mechanism by which deforestation causes the enhanced ENSO variability and mean state changes begins with the effects on surface temperature, with the deforested regions experiencing warmer surface temperatures. The surface warming leads to changes in the surface winds which extend

well into the Pacific and Atlantic, and affect in particular the annual mean wind stress on the ocean, with westerly anomalies in the far eastern Pacific and easterlies in the Atlantic. In the Pacific, the westerly anomalies lead to warm SST anomalies, probably due to reduced upwelling. These anomalies are amplified and modified by coupled feedbacks, and the coupled ocean-atmosphere system responds with warming in the annual mean SST in the eastern equatorial Pacific, a state which is more unstable to ENSO SST variability in this CGCM.

The properties of the wind stress changes produced directly by the deforestation which are responsible for the changes in the coupled climate are not obvious by inspection. Experiments with an ICM indicate that the key region in which the wind stress is influenced by the deforestation may be close to the NINO1 region, possibly extending eastward to the South American coast. The simplest models (Fedorov and Philander 2001) do not address the structures found in the AGCM simulation. It is possible that the stability results could be model dependent. It would therefore be interesting to repeat the deforestation experiment with other CGCMs. Also, Amazon deforestation may be leading to strong seasonal effects in the CGCM that have not been addressed due to considering only the annual mean. These should be documented and analyzed.

The CGCM suffers from substantial biases in both the ENSO simulation and the climatology in the Amazon regions, so that results presented here may not be generalizable to other CGCMs. Our diagnosis indicates that the effects of Amazon deforestation in warming the local surface temperature and reducing precipitation produce responses of opposite sign on the zonal wind stress in the eastern equatorial

Pacific, and that the surface temperature effect wins out. If the CGCM climatology in the Amazon region was more realistic (cooler and wetter), the response to the precipitation anomalies could become relatively more important, potentially leading to results of opposite sign.

We speculate that the mechanism described in this paper could be relevant to some outstanding problems. First is the problem of biases in the tropical SST simulations of CGCMs. Warm SST in the eastern tropical Pacific along the South American coast is a well known bias (e.g. Davey et al., 2001), as is cold SST in the western tropical Pacific, and too little precipitation over the Amazon is also frequently found. A similar SST bias is also common in the Atlantic (Davey et al., 2001): warm along the African coast and cold in the western equatorial Atlantic. The warm bias is highly asymmetric about the equator, with maximum bias to the south. If there was a warm bias in the land surface temperature in the adjacent continental area, this could contribute to the warm bias in the SST by inducing westerlies in the eastern oceans as in Fig. 6b, warming the SST by reducing upwelling, with subsequent coupled feedbacks. On the other hand, the opposite effect could occur in the ocean on the eastern side of the warm land, possibly leading to cold biases in the western equatorial ocean basins (e.g. Fig. 3c). That is, tropical biases over land could be in part responsible for tropical biases in SST in CGCMs. The strength of this mechanism could be tested by artificially cooling tropical land surface temperatures, for example by applying a flux correction over land. While the magnitude of the eastern tropical Pacific warming in our deforestation experiments is small compared to the biases, it should be remembered that the mean ocean state of our model is constrained by a strong form of flux correction.

Another interesting phenomenon is the El Niño-like warming found in some CGCM simulations of greenhouse warming. It is well known that simulated warming at a constant longitude tends to be larger over land than over ocean in greenhouse warming simulations. This phenomenon occurs at all latitudes. The El Niño-like warming could then be a consequence of westerlies in the eastern tropical Pacific forced by the preferential warming in tropical South America.

*Acknowledgments***.** This research was supported by grants from the National Science Foundation ATM-0332910, the National Oceanic and Atmospheric Administration NA04OAR4310034, and the National Aeronautics and Space Administration NNG04GG46G.

References

Bhatt, U. S., E. K. Schneider, and D. G. DeWitt, 2002: Impact of North American soil moisture variability on the re-emergence of SST anomalies in the North Atlantic. *Global and Planetary Change*, **37**, 33-56.

Briegleb, B. P., 1992: Delta-Eddington approximation for solar radiation in the NCAR Community Climate Model. *J. Geophys. Res.*, **97**, 7603-7612.

Clement, A. C., Cane, M. A., Seager, R., 2001: An orbitally driven tropical source for abrupt climate change, *J. Climate* 2001, **14**, 2369-2375.

Davey, M. K., and Coauthors, 2001: STOIC: A study of coupled model climatology and variability in tropical ocean regions. *Climate Dyn.*, **18**, 403-420.

Delire, C., P. Behling, M. Coe, J. Foley, R. Jacob, J. Kutzbach, Z. Liu, and S. Vavrus, 2001: Simulated response of the atmosphere-ocean system to deforestation in the Indonesian Archipelago. *Geophys. Res. Lett.*, **28**, 2081-2084.

DeWitt, D. G., 1996: The effect of the cumulus convection scheme on the climate of the COLA general circulation model. COLA Rep. 27, 58 pp. [Available from COLA, 4041 Powder Mill Rd., Suite 302, Calverton, MD 20705.]

DeWitt, D. G., E. K. Schneider, and A. D. Vernekar, 1996: Factors determining the precipitation distribution and low-level flow in the tropics of an atmospheric general circulation model: Diagnostic studies. *J. Atmos. Sci.*, **53**, 2247-2263.

DeWitt, D. G., and E. K. Schneider, 1996: The Earth radiation budget as simulated by the COLA GCM. COLA Rep. 35, 39pp. [Available from COLA, 4041 Powder Mill Rd., Suite 302, Calverton, MD 20705.]

Dickinson, R. E., and A. Henderson-Sellers, 1988: Modelling tropical deforestation: A study of GCM land-surface parameterizations. *Quart. J. Roy. Meteor. Soc.*, **114**, 439-462.

Dirmeyer, P. A., and J. Shukla, 1994: Albedo as a modulator of climate response to tropical deforestation. *J. Geophys. Res*., **99**, 20863-20877.

Dirmeyer, P. A., and F. J. Zeng, 1999: An update to the distribution and treatment of vegetation and soil properties in SSiB. *COLA Technical Report 78* [Available from the Center for Ocean-Land-Atmosphere Studies, 4041 Powder Mill Road, Suite 302, Calverton, MD 20705 USA], 25 pp.

Fedorov, A.V., and Philander, S.G.H. 2001: A stability analysis of tropical Ocean-Atmosphere Interactions (Bridging Measurements of, and Theory for El Niño). *J. Climate*, **14**, 3086-3101.

Flügel, M., P. Chang and C. Penland. 2004: The Role of Stochastic Forcing in Modulating ENSO Predictability. *J. Climate*, **17**, 3125–3140.

Gent, P. R., and J. C. McWilliams, 1990: Isopycnal mixing is ocean circulation models. *J. of. Phys. Oceanography*, **25,** 150-155.

Gill, A. E., 1980: Some simple solutions for heat-induced tropical circulation. *Quart. J. Roy. Meteor. Soc.*, **106**, 447-462.

Goldenberg, S. B., and J. J. O'Brien, 1981: Time and space variability of the tropical Pacific wind stress. *Mon. Wea. Rev.*, **109**, 1190-1207.

Harshvardhan, R. Davies, D. A. Randall and T. G. Corsetti, 1987: A fast radiation parameterization for atmospheric circulation models. *J. Geophys. Res.*, **92(D1)**, 1009-1016.

Henderson-Sellers, A., and V. Gornitz, 1984: Possible climatic impacts of land cover transformations, with particular emphasis on tropical deforestation. *Clim. Change*, **6**, 231-258.

Hu, Z.-Z., E. K. Schneider, U. S. Bhatt, and B. P. Kirtman, 2004: Potential for influence of land surface processes on ENSO. *J. Geophys. Res.*, **109**, D21113, doi:10.1029/2004JD004771.

Jin, F. F., and Neelin J. D., 1993a: Modes of interannual tropical ocean–atmosphere interaction—A unified view. Part I: Numerical results. *J. Atmos. Sci.,* **50**, 3477–3503.

Jin, F. F., and Neelin J. D., 1993b: Modes of interannual tropical ocean–atmosphere interaction—A unified view. Part III: Analytical results in fully coupled cases. *J. Atmos. Sci.,* **50**, 3523-3540.

Kiehl, J. T., J. J. Hack and B. P. Briegleb, 1994: The simulated Earth radiation budget of the National Center for Atmospheric Research community climate model CCM2 and comparisons with the Earth Radiation Budget Experiment (ERBE). *J. Geophys. Res.*, **99**, 20815-20827.

Kiehl, J. T., J. J. Hack, G. Bonan, B. A. Boville, D. L. Williamson, and P. J. Rasch, 1998: The National Center for Atmospheric Research Community Climate Model: CCM3. *J. Climate,* **11,** 1131–1149.

Kirtman, B. P., 1997: Oceanic Rossby wave dynamics and the ENSO period in a coupled model. *J. Climate*, **10**, 1690-1704.

Kirtman, B. P., and J. Shukla, 2002: Interactive coupled ensemble: A new coupling strategy for CGCMs. Geophys. Res. Lett., 29, 1367, doi: 10.1029/2002GL014834.

Kirtman, B. P., J. Shukla, B. Huang, Z. Zhu and E. K. Schneider, 1997: Multiseasonal predictions with a coupled tropical ocean global atmosphere system. *Mon. Wea. Rev.,* **125**, 789-808.

Kirtman, B. P., Y. Fan and E. K. Schneider, 2002: The COLA global coupled and anomaly coupled ocean-atmosphere GCM. *J. Climate,* **15**, 2301-2320.

Kirtman, B. P., K. Pegion and S. M. Kinter, 2005: Internal Atmospheric Dynamics and Tropical Indo-Pacific Climate Variability. *J. Atmos. Sci.*, **62**, 2220-2233.

Large, W. G., J. C. McWilliams, and S. C. Doney, 1994: Oceanic vertical mixing: A review and a model with a nonlocal boundary layer parameterization. *Rev. of Geophys.*, **32,** 363-403.

Latif, M., K. Sperber, et al., 2001: ENSIP: the El Nino simulation intercomparison project. *Climate Dynamics*, **18**, 255-276.

Lindzen, R. S. and S. Nigam, 1987: On the role of sea surface temperature gradients in forcing low-level winds and convergence in the Tropics. *J. Atmos. Sci.*, **44**, 2418-2436.

Marx, L., 2001: New Astronomy in the COLA Atmospheric General Circulation Model. COLA Tech. Rept. 93, 27pp. [Available from COLA, 4041 Powder Mill Rd., Suite 302, Calverton, MD 20705.]

Meehl, G. A., and W. M. Washington, 1996: El Nino-like climate change in a model with increased atmospheric CO_2-concentration. *Nature*, **382**, 56-60.

Mellor, G. L., and T. Yamada, 1982: Development of a turbulence closure model for geophysical fluid processes. *Rev. Geophys. Space Phys.*, **20**, 851-875.

Misra, V., P. A. Dirmeyer, and B. P. Kirtman, 2003: Dynamic downscaling of seasonal simulations over South America. *J. Climate*, **16**, 103-117.

Miyakoda, K., and J. Sirutis, 1977: Comparative integrations of global spectral models with various parameterized processes of subgrid scale vertical transports. *Beitr. Phys. Atmos.,* **50,** 445–480.

Moorthi, S., and M. J. Suarez, 1992: Relaxed Arakawa-Schubert: A parameterization of moist convection for general circulation models. *Mon. Wea. Rev.*, **120**, 978-1002.

Neelin, J. D., 1989: On the interpretation of the Gill model. *J. Atmos. Sci.*, **46**, 2466-2468.

Nobre, C. A., P. J. Sellers, and J. Shukla, 1991: Amazonian deforestation and regional climate change. J. Climate, 4, 957-988.

Pacanowski, R. C., and S. M. Griffies, 1998: MOM 3.0 Manual, NOAA/Geophysical Fluid Dynamics Laboratory, Princeton, USA 08542.

Rayner, N. A., E. B. Holton, D. E. Parker, C. K. Folland, and R. B. Hackett (1996), Global Sea-Ice and Sea Surface Temperature data set, 1903-1994, Version 2.2, Hadley Center for Climate Prediction and Research Tech. Note 74, Met Office, Bracknell, Berkshire, United Kingdom.

Redi, M. H., 1982: Oceanic isopycnal mixing by coordinate rotation, *J. of Phys. Oceanogr*., **12**, 1155-1158.

Ropelewski, C. F., J. E. Janowiak, and M. F. Halpert, 1985: The analysis and display of real time surface climate data. *Mon. Wea. Rev*., **113**, 1101-1107.

Schneider, E. K., 2002: Understanding differences between the equatorial Pacific as simulated by two coupled GCMs. *J. Climate*, **15**, 449-469.

Schneider, E. K. and R. S. Lindzen, 1976: The influence of stable stratification on the thermally driven tropical boundary layer. *J. Atmos. Sci.*, **33**, 1301-1307. Corrigendum, *J. Atmos. Sci.*, **33**, 1827.

Schopf, P. S. and R. Burgman, 2006: A simple mechanism for ENSO residuals and asymmetry. *J. Climate*, **19**, 3167-3179.

Smagorinsky, J., 1963: General circulation experiments with the primitive equations: I. The basic experiment. *Mon. Wea. Rev.,* **91,** 99-164.

Smith, T. M., R. W. Reynolds, R. E. Livezey, and D. C. Stokes, 1996: Reconstruction of historical sea surface temperature using empirical orthogonal functions. *J. Climate,* **9,** 1403–1420.

Sud, Y. C., G. K. Walker, J.-H. Kim, G. E. Liston, P. J. Sellers, and W. K.-M. Lau, 1996: Biogeophysical consequences of a tropical deforestation scenario: A GCM simulation study. *J. Climate*, **9,** 3225-3247.

Trenberth, K. E., W. G. Large, and J. G. Olson, 1990: The mean annual cycle in global ocean wind stress. *J. Phys. Oceanogr.*,**20,** 1742–1760.

Voldoire, A., and J.-F. Royer, 2005: Climate sensitivity to tropical land surface changes with coupled versus prescribed SSTs. *Climate Dyn.*. doi:10.1007/s00382-005-0014-7.

Wu, Z., E. K. Schneider, and B. P. Kirtman, 2004: Causes of low frequency North Atlantic SST variability in a coupled GCM. *Geophys. Res. Lett.*, **31**, L09210, doi:10.1029/2004GL019548.

Xie, P., and P. Arkin, 1996: Analyses of global monthly precipitation using gauge observations, satellite estimates, and numerical model predictions. *J. Climate*, **9**, 840-858.

Xue, Y., P. J. Sellers, J. L. Kinter III, and J. Shukla, 1991: A simplified biosphere model for global climate studies. *J. Climate*, **4,** 345–364.

Xue, Y., F. J. Zeng, and C. A. Schlosser, 1996: SSiB and its sensitivity to soil properties - a case study using HAPEX-Mobilhy data. *Global and Planetary Change*, **13**, 183-194.

Zeng, N., and J. D. Neelin, 1999: A land-atmosphere interaction theory for the tropical deforestation problem. J. Climate, 12, 857-872.

Zebiak, S. E., and M. A. Cane, 1987: A model of El Niño and Southern Oscillation. *Mon. Wea. Rev.*, **115**, 2262-2278.

Table 1. Experiments

Experiment Name	Description
CONTROL	CGCM control (100 years)
DEFOREST	CGCM Amazon deforestation (100 years)
WIND	Annual mean wind stress anomalies from AGCM-only Amazon deforestation simulation added to CGCM with CONTROL vegetation (40 years)

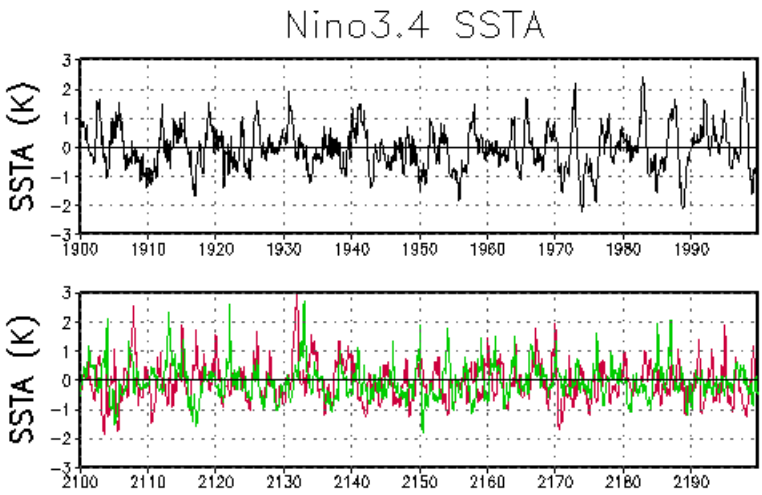

Figure 1. NINO3.4 (170°W-120°W, 5°S-5°N) SSTA. Top: observed (top); bottom: CONTROL (green), and DEFOREST (red) simulations.

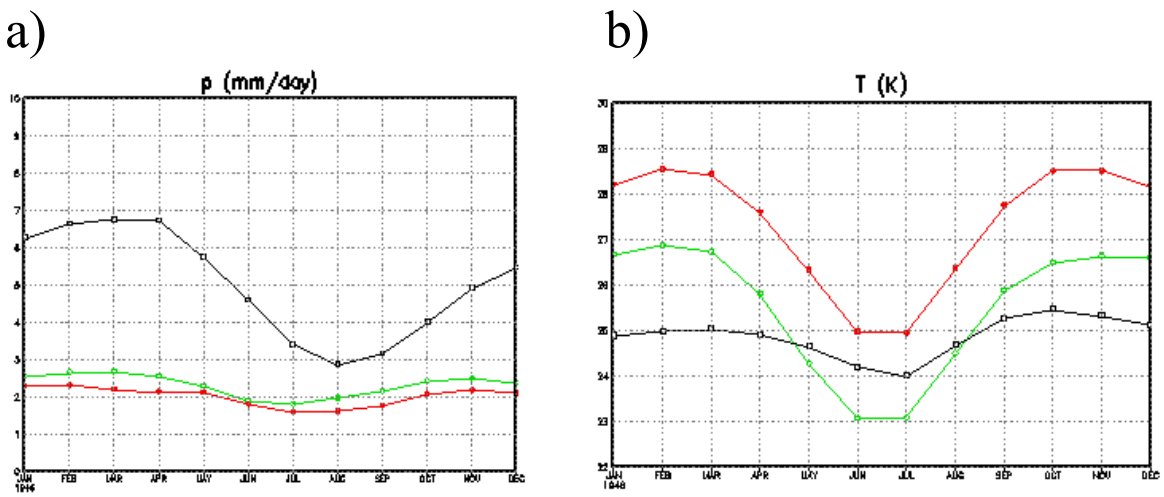

Figure 2. Climatological means over land from 80°W-40°W and 15°S-8°N. which contains the deforested region for analysis (black), CONTROL (green), and DEFOREST (red). (a) Precipitation (mm day^{-1}). (b) Surface temperature (K).

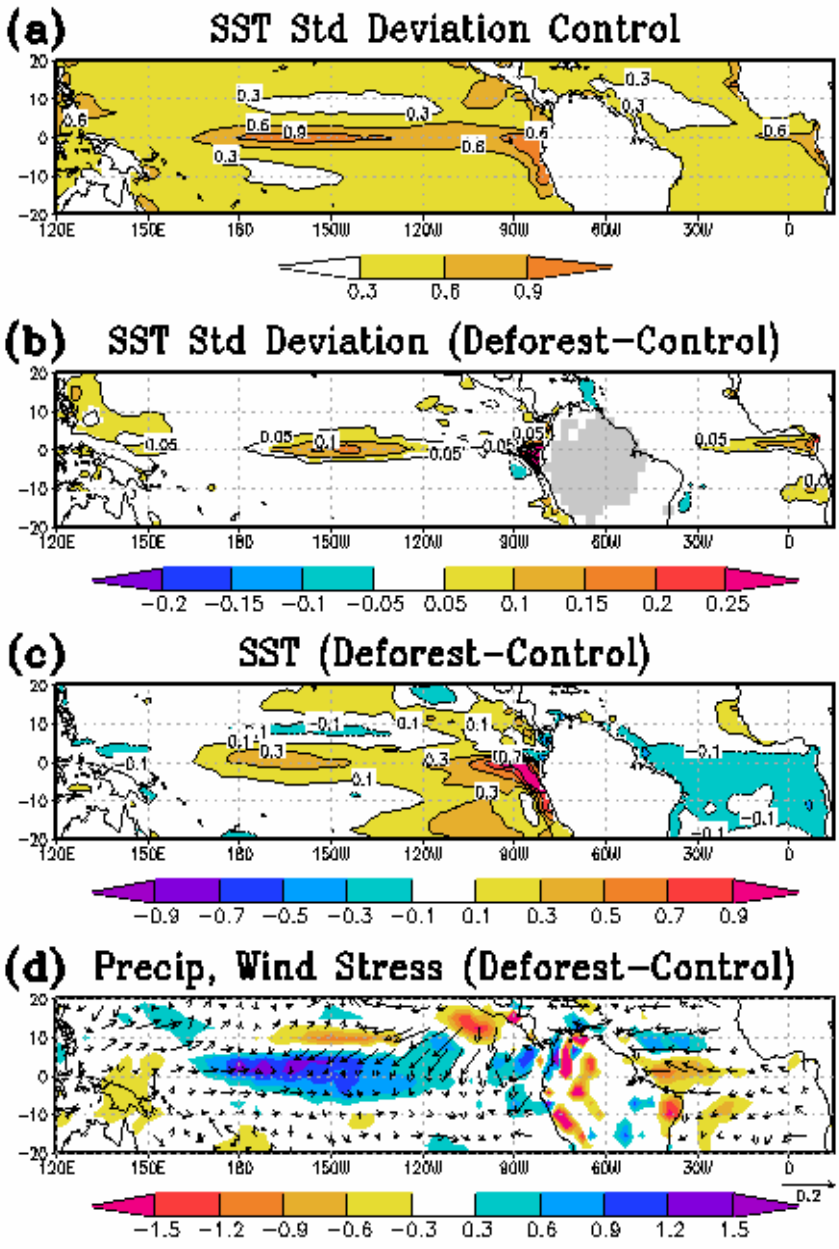

Figure 3. Effects of Amazon deforestation on the coupled climate from 100 years of simulation. (a) Standard deviation of CONTROL SST anomalies (°C). (b) Difference of standard deviations of SST anomalies, DEFOREST minus CONTROL. Colored regions are significant at the 5% level. Deforested region is indicated in grey. (c) Annual mean SST difference (°C), DEFOREST minus CONTROL. (d) Difference in annual mean precipitation (shaded, mm day^{-1}) and wind stress on the ocean (vectors, dynes cm^{-2}), DEFOREST minus CONTROL.

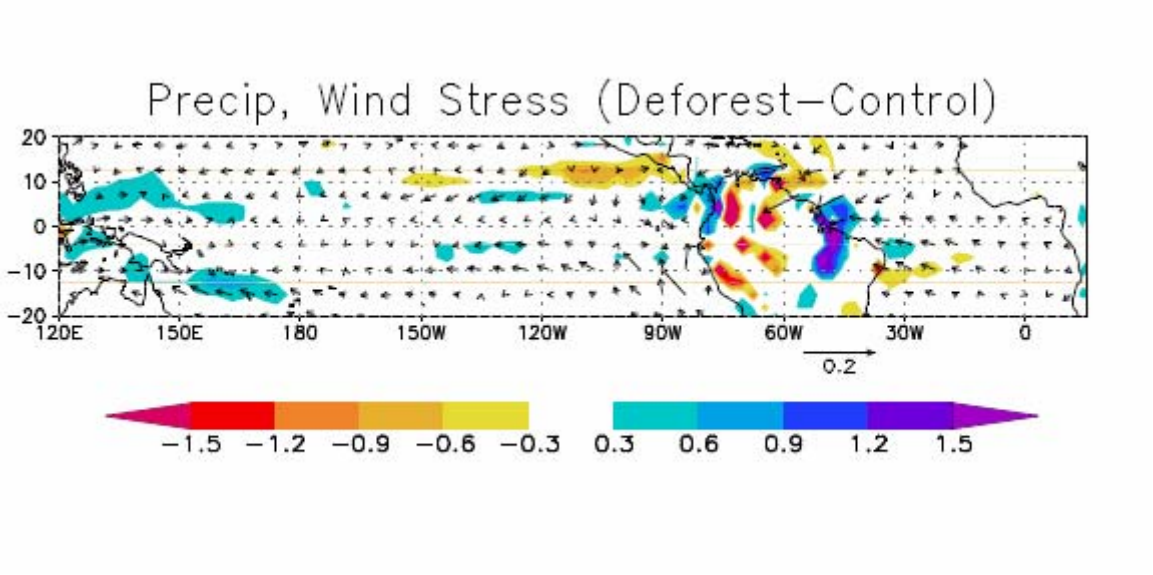

Figure 4. Annual mean effects of Amazon deforestation (deforestation minus control) in AGCM simulations with specified climatological SST. Precipitation (, shaded, mm day^{-1}) and wind stress on the ocean (vectors, dynes cm^{-2}).

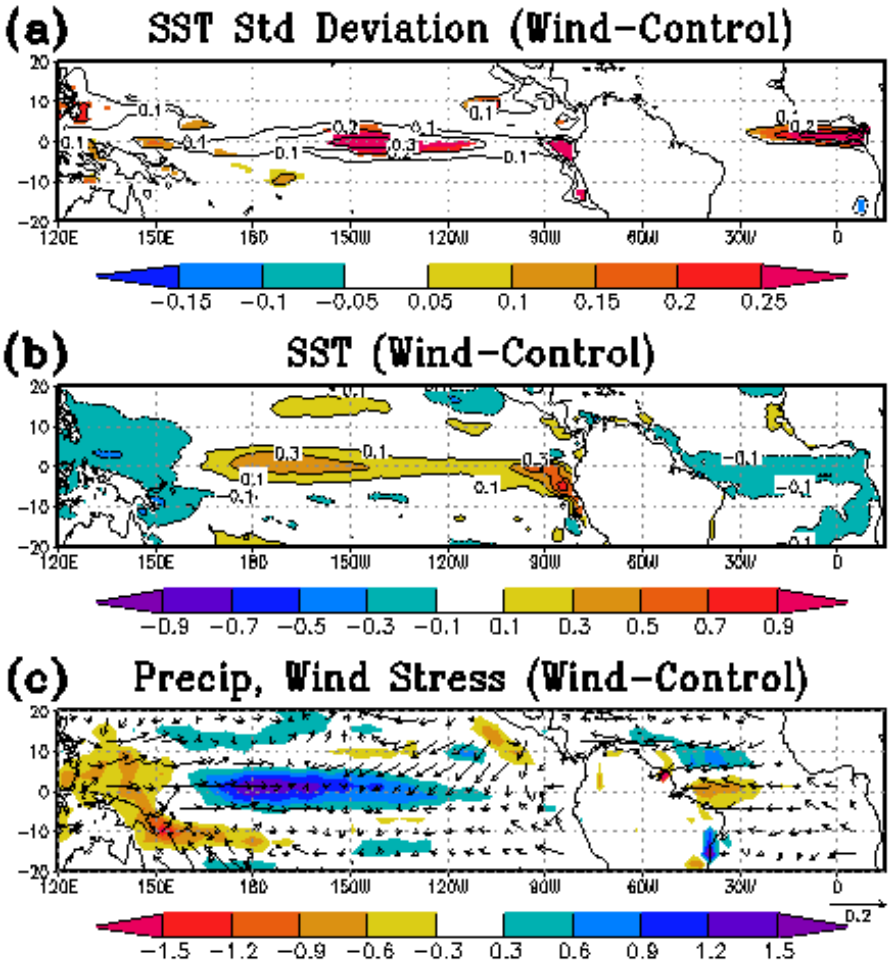

Figure 5. Sensitivity of the coupled climate to addition of the wind stress anomaly from Fig. 4 in 30 years of simulation WIND, demonstrating that the origins of the oceanic impacts of deforesting the region shown in Fig. 3b are contained in the mean wind stress differences of the AGCM only simulations. (a) Difference of standard deviations of SST anomalies. Colored regions are significant at the 5% level. (b) Annual mean SST difference (°C). (d) Difference in annual mean precipitation (shaded, mm day^{-1}) and wind stress on the ocean (vectors, dynes cm^{-2}).

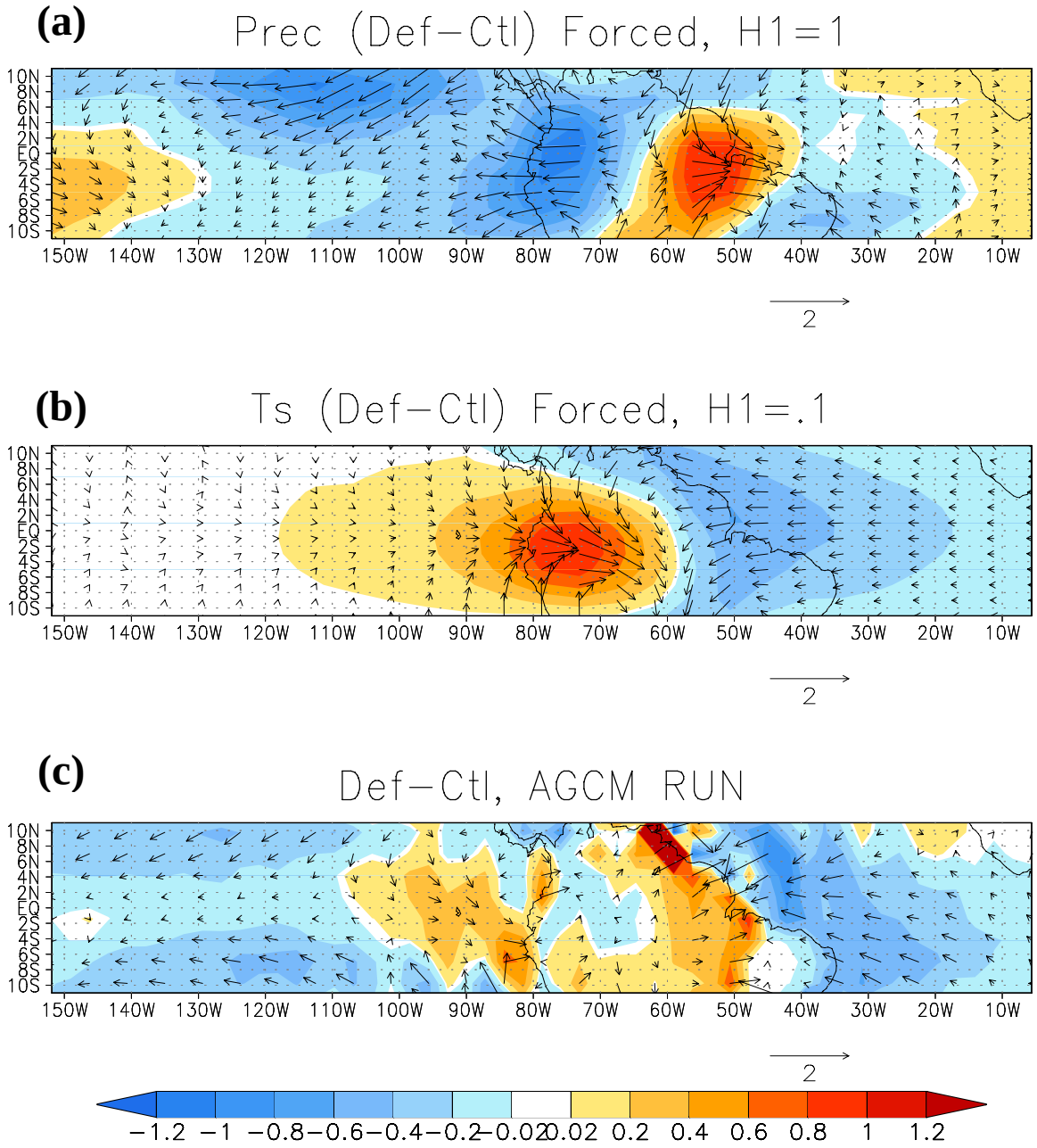

Figure 6. Scaled surface wind response, deforest minus control, of simple Gill-type model to forcing obtained from the AGCM-only simulations with specified climatological SST. (a) Forcing by precipitation anomalies shown in Fig. 4, representing atmospheric heating. (b) Forcing by land surface temperature anomalies. (c) Response from AGCM simulations. Shading represents the zonal component. See text for details.